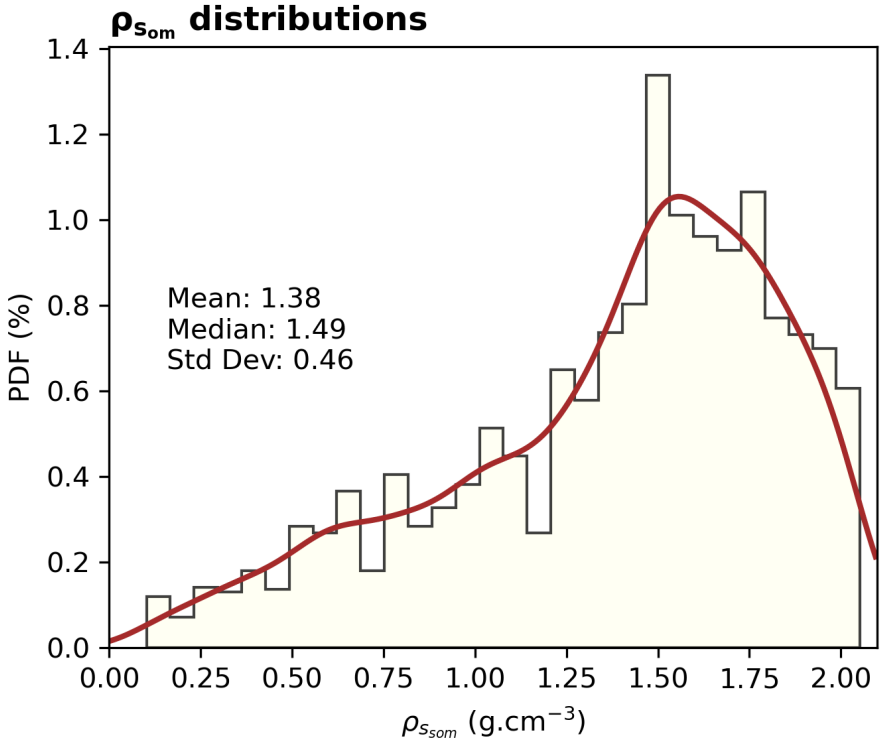

Figure S3. Distribution of organic matter particle density ($\rho_{s_{om}}$, g cm^{-3}) across the compiled datasets. The histogram (bars) is shown with a kernel density estimate (red line). The mean, median, and standard deviation are indicated in the panel.

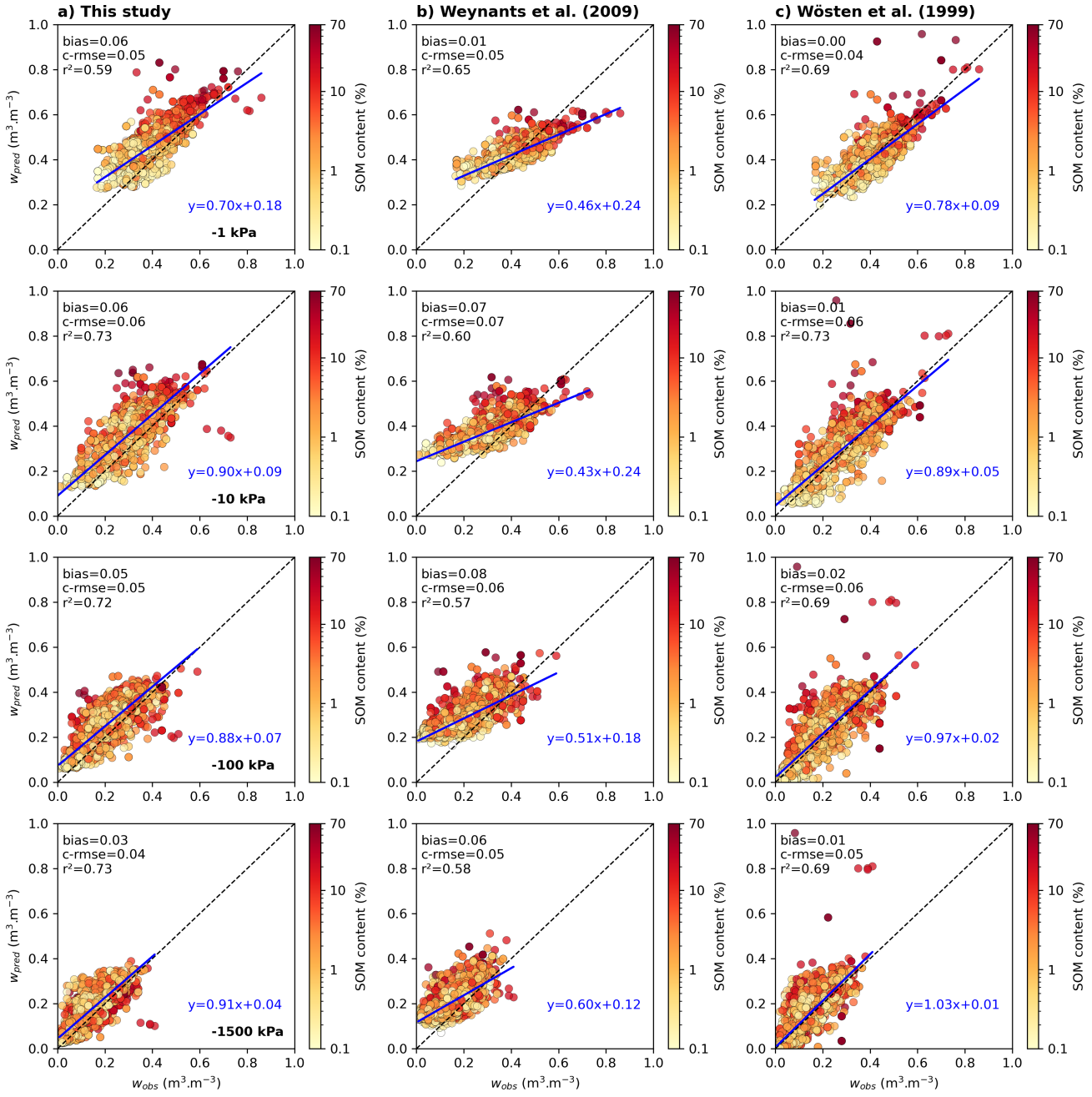

Figure S4. As Figure 6, but including the comparison of the PTFs of Weynants et al. (2009) and Wösten et al. (1999) with the dataset from Kristensen et al. (2019). Panels show the predicted versus observed volumetric water content at different matric potentials (-1, -10, -100, and -1500 kPa) for (a) this study, (b) Weynants et al. (2009), and (c) Wösten et al. (1999).

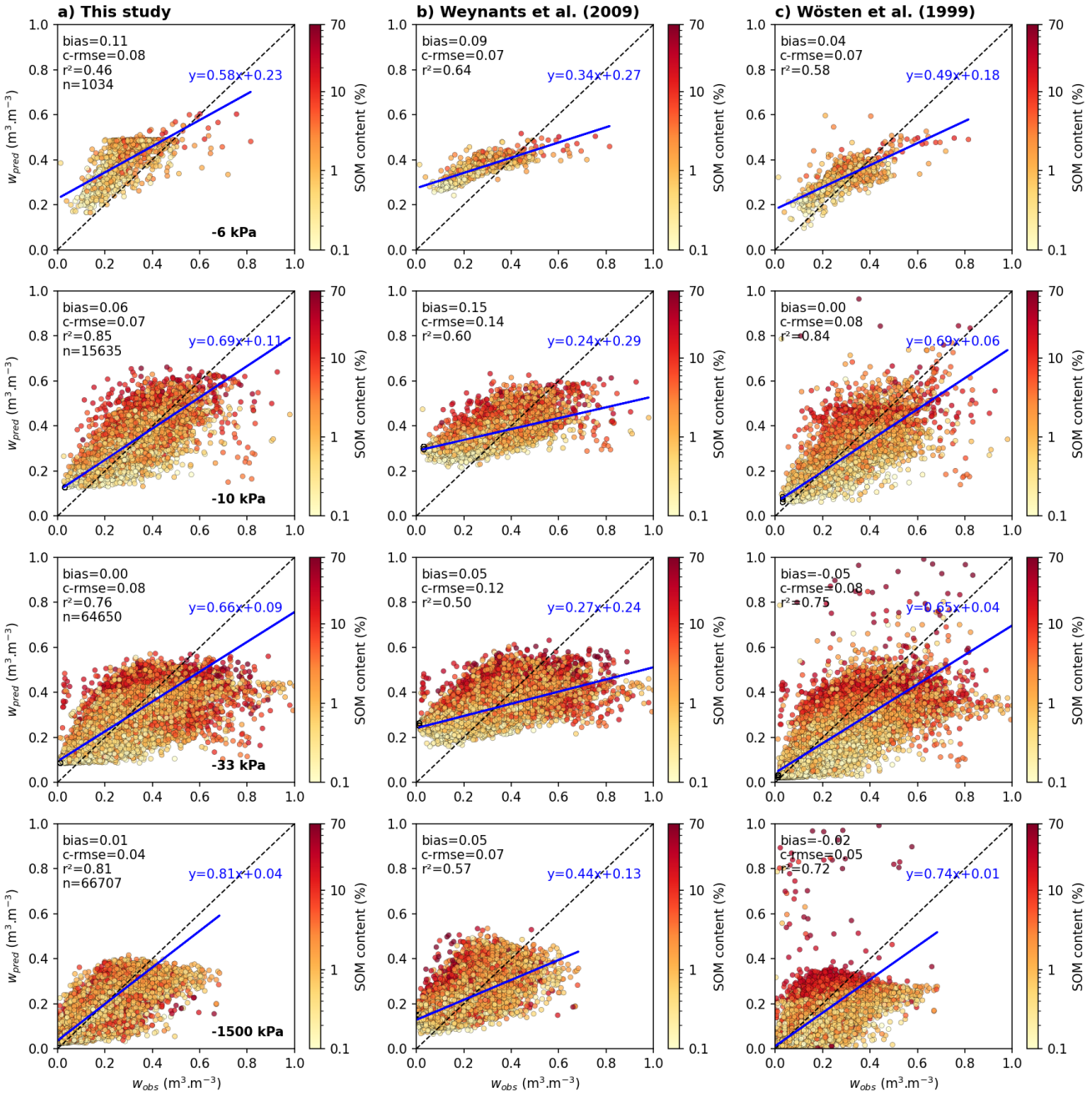

Figure S5. As Figure 7, but including the comparison of the PTFs of Weynants et al. (2009) and Wösten et al. (1999) with the dataset from Gupta et al. (2021). Panels show the predicted versus observed volumetric water content at different matric potentials (-6, -10, -33, and -1500 kPa) for (a) this study, (b) Weynants et al. (2009), and (c) Wösten et al. (1999).

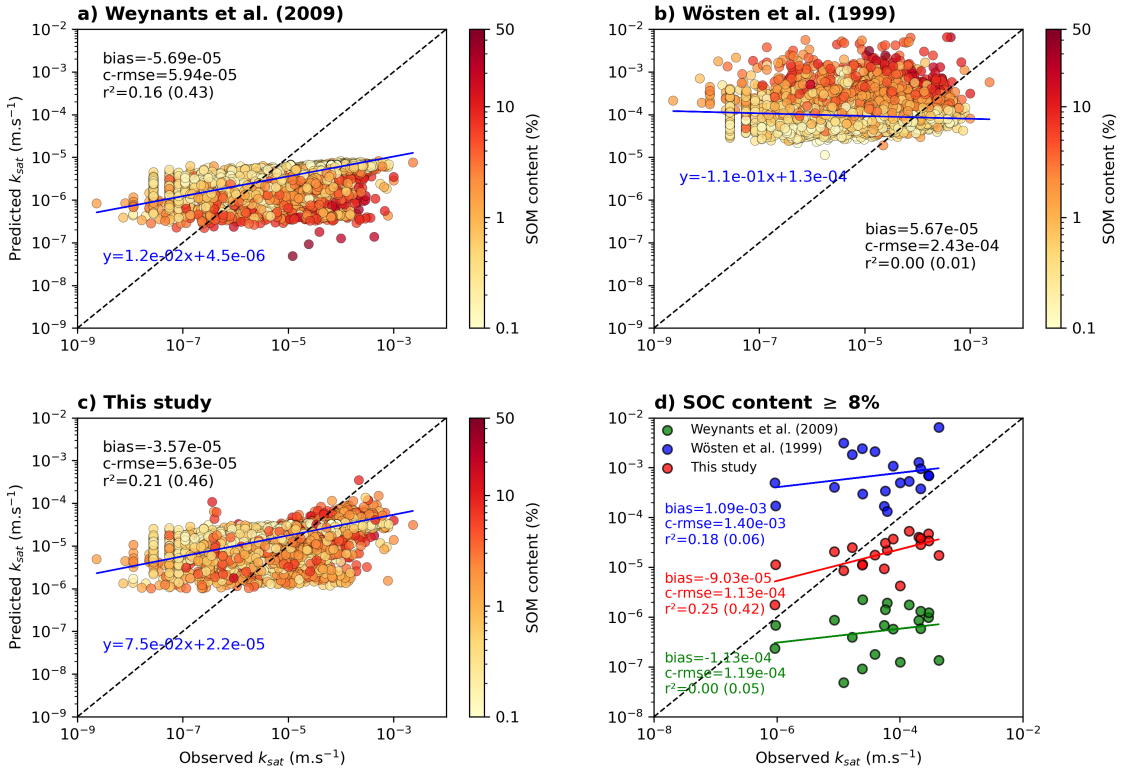

Figure S6. As Figure 8, but including the comparison of the PTFs of Weynants et al. (2009) and Wösten et al. (1999) with the dataset from Gupta et al. (2021). Panels show the predicted versus observed saturated hydraulic conductivity for (a) Weynants et al. (2009), (b) Wösten et al. (1999), (c) this study, and (d) soils with SOC content $\geq$ 8%.